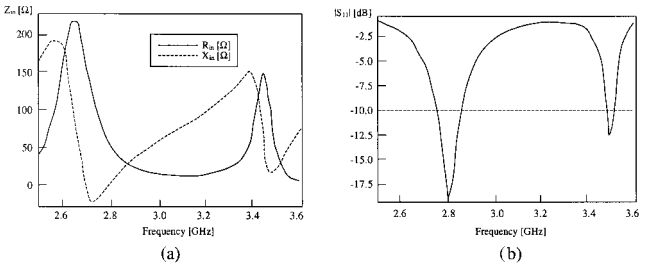

Figure 5 (a) Input impedance, and (b) reflection coefficient amplitude, for the antenna shown in Figure 4

convergence has been firstly tested. A 5 cm × 5 cm centred probe (inner radius: 5 mm) fed patch has been used as test structure and the input impedance variation as a function of the number of unknowns has been considered. The obtained results are reported in Figure 2.

In Figure 2 the input resistance behaviour has been omitted since relative errors are much smaller than in the reactance case. It can be seen that for a number of 12 × 10 rectangular domains and 8 basis functions for the probe, the relative errors are below 1% on the input reactance (while they are below 0.1% on the input resistance). These error values are usually acceptable for a wide family of applications.

The numerical code has been then applied to synthesis problems when prescribed resonant frequencies are given. We present a dual-band antenna design starting from the mother geometry of Figure 3(a) as follows. Using 227 unknowns in the MoM code, the resulting input impedance is reported in Figure 3(b). Starting from this layout, the numerical code has been asked to find a dual-band patch shape at 2.8 and 3.5 GHz. The resulting shape obtained with a populations of 100 individuals, and the GA search steps are reported in Figure 4 (for each generation best individual fitness is shown).

Figure 5 shows the input impedance and the reflection coefficient amplitude at the input port for the antenna depicted therein. The given requirements have been completely fulfilled.

If the patch shape had to be found without GA, checking one by one all the possible shapes, the number of linear systems to solve would have amounted to 17 million. Using GA, instead, only 3400 linear systems have been solved and the time employed was only 0.02% of the time needed to solve the entire system set.

IV. CONCLUSIONS

A numerical code for multifrequency antenna design has been presented in this paper. This code employs MoM and GA to find the optimal patch shape, starting from a rectangular geometry discretized with a user-chosen detail level. The entire synthesis process is wholly automatic, allowing a user of whatever skill level to carry out satisfactory multifrequency designs.

REFERENCES

1. F. Bilotti and C. Vegni, Rigorous and Efficient Full-Wave Analysis of Trapezoidal Patch Antennas, IEEE Trans Antennas Propagat AP-49 (2001), 1773–1776.
2. C. Vegni and F. Bilotti, Parametric Analysis of Slot-Loaded Trapezoidal Patch Antennas, IEEE Trans Antennas Propagat AP-50 (2002).
3. F. Bilotti and C. Vegni, Patch Antennas with Convex Polygonal Shape, Proc Int Conf Electromag Adv Applic (ICEAA '01), Torino, Italy, (2001), 485–488.
4. J.M. Johnson, Y. Rahmat-Samii, Genetic Algorithms and Method of Moments (GA/MOM) for the Design of Integrated Antennas, IEEE Trans Antennas Propagat AP-47 (1999), 1606–1614.
5. J.R. Mosig and F.E. Gardiol, General Integral Equation Formulation for Microstrip Antennas and Scatterers, Proc IEEE 132 (1985), 424–432.
6. S.M. Rao, D.R. Wilton, and A.W. Glisson, Electromagnetic Scattering by Surfaces of Arbitrary Shape, IEEE Trans Antennas Propagat AP-30 (1982), 409–418.
7. D.E. Goldberg, Genetic Algorithms in Search, Optimization and Machine Learning, Addison-Wesley, Reading, MA, 1989.

A PHYSICAL APPROACH TO GENERATING TIME FREQUENCY DISTRIBUTIONS OF DYNAMIC CEM TARGETS

M. Carr and J. L. Volakis
Radiation Laboratory, Electrical Engineering and Computer Science
University of Michigan, Ann Arbor, MI 48109-2122

Received 29 April 2002

ABSTRACT: *Generating accurate, high-resolution time-frequency distributions (TFD) is a critical aspect of dynamic radar scattering analysis. Well-formed TFD's can be used for target identification, target acquisition in high-noise environments, or extending the range of radar systems. In this paper, we diverge from traditional methods employing complex signal-processing methods and propose a simple approach for constructing the TFD for computational electromagnetic (CEM) targets based on the physics of the problem. The proposed method allows for an arbitrarily high resolution at any single look angle. Several examples are presented to validate the method.* © 2002 Wiley Periodicals, Inc.
Microwave Opt Technol Lett 35: 186–189, 2002; Published online in Wiley InterScience (www.interscience.wiley.com). DOI 10.1002/mop.10552

Key words: *time-frequency; radar; computational electromagnetics; moment method; Doppler*

1. INTRODUCTION

The Fourier Transform has long been an important tool for providing a measure of the frequencies contained within a signal. Time-frequency distributions (TFD) extend the functionality of the Fourier Transform by computing the localized frequency content at a particular time within the signal. Thus, one can obtain information about the dynamic frequency-domain behavior of a signal over time. Within the realm of radar scattering, one can interpret the TFD physically as a representation of the dynamically changing Doppler frequency shifts caused by moving targets or targets with moving components. TFDs can then be used for a variety of applications, such as clutter reduction and moving target detection using airborne radars [1].

As an example, consider the $\hat{z}$-directed dipole source spinning about the origin as shown in Figure 1(a), where we wish to measure the far field radiated in the negative $\hat{x}$-direction [2]. From Doppler theory, we know that the frequency measured at the observation point will shift upwards when the source is approaching the observer. As the source recedes, the observed frequency shifts downward with the Doppler shift frequency given by

$$f_D = -2\frac{\mathbf{v}\cdot\hat{x}}{\lambda}. \tag{1}$$

Since $\mathbf{v} = 2\pi l\hat{\phi}(t)$, where $\hat{\phi}$ is the usual cylindrical unit vector and t denotes time, the Doppler frequency as time increases can then be expressed as

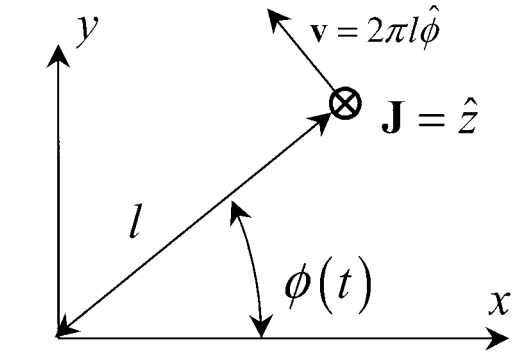

(a)

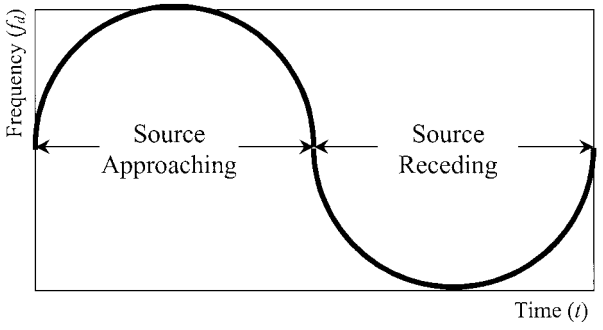

(b)

Figure 1 (a) Z-directed dipole source spinning about the origin. (b) TFD representation of the radiated field in the negative x-direction

$$f_D = -4\pi l \frac{\hat{\phi}(t) \cdot \hat{x}}{\lambda} = \frac{4\pi l \sin(t)}{\lambda}. \tag{2}$$

A TFD of this situation would then look as that shown in Figure 1(b).

In practice, to generate Figure 1(b) we use the scattered signal from the rotating object. The simplest and most well known method for generating a given signal's TFD is the windowed Fourier transform known as the spectrogram [3]. Basically, to find the signal component associated with frequency ω at a certain time t, the received signal $s(t')$ is multiplied by a windowing function $h(t')$ centered at time t. The result is then transformed to frequency domain to yield

$$S_t(\omega) = \frac{1}{\sqrt{2\pi}} \int e^{-j\omega t'} s(t') h(t' - t)\, dt'. \tag{3}$$

Here $S_t(\omega)$ is the spectrum of the windowed signal at time t. From Eq. (3), it is evident that a compact windowing function h will increase localization in time domain but lower resolution in frequency domain. Conversely, a wide windowing function will lead to high frequency resolution and low time localization. This uncertainty principle, present in all signal-processing TFD approaches, ultimately limits our overall resolution and forces us to settle for a compromise between time and frequency resolution. It is, of course, desirable to remove this restriction and allow for an arbitrary resolution in both domains.

In proceeding to remove such a restriction, we note that Eq. (3) neglects information from the individual currents **J**, which are the source of the scattered field (see Fig. 2(a)). In this paper we present a physics-based approach called the Direct TFD (DTFD) for computing each column of the TFD from knowledge of the individual currents upon the geometry and its velocity at a single look angle. In this manner, the intermediate calculation of the scattered field is bypassed (see Fig. 2(b)), thus avoiding the uncertainty principle and allowing for much higher resolution. Further, DTFD has **O**(N) complexity and requires little memory.

2. DIRECT TFD FORMULATION

Computation of the scattered fields (as required for signal-processing methods) requires lumping all induced currents into a single field value, therefore forfeiting much detail about the target's electromagnetic characteristics. In the DTFD method, we instead use information about the geometry's instantaneous velocity to localize (in frequency) the contribution from each current source. From Doppler theory, we know that the velocity of the geometry upon which the source resides will determine the apparent frequency shift as seen by a stationary observer. We can also account for any frequency shift of the induced currents due to the geometry's motion through the incident field by expressing the localized current as

$$\mathbf{J}'(\mathbf{r}, f_d) = \mathbf{J}(\mathbf{r})\delta\left[f_d - \frac{\hat{r}_s \cdot \mathbf{v}(\mathbf{r})}{\lambda} - \frac{\hat{r}_o \cdot \mathbf{v}(\mathbf{r})}{\lambda}\right] \tag{4}$$

where δ is the Dirac delta function, λ is the carrier wavelength, f_d is the Doppler frequency shift, $\hat{r}_o$ and $\hat{r}_s$ are unit vectors in the direction of the observer and source, respectively, and $\mathbf{v}(\mathbf{r})$ is the velocity of the geometry at point $\mathbf{r}$. For the monostatic case, $\hat{r}_o = \hat{r}_s$ and thus Eq. (4) simplifies to

$$\mathbf{J}'(\mathbf{r}, f_d) = \mathbf{J}(\mathbf{r})\delta\left[f_d - 2\frac{\hat{r}_o \cdot \mathbf{v}(\mathbf{r})}{\lambda}\right] \tag{5}$$

By modifying the currents as shown, we restrict the radiation integral to include only those currents which appear at a given Doppler shift f_d, and thus extend our usual computation of the

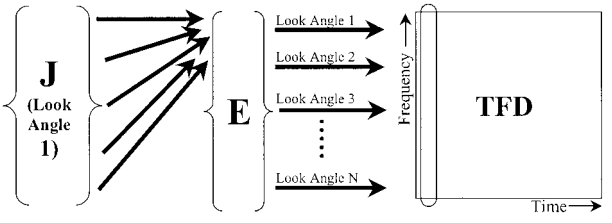

(a)

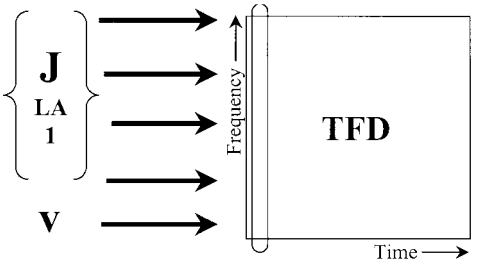

(b)

Figure 2 (a) Standard signal-processing methods such as the spectrogram. (b) The proposed Direct TFD (DTFD) method

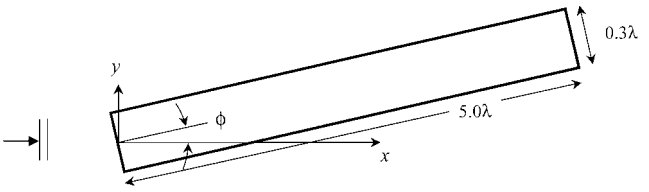

Figure 3 A 5.0λ × 0.3λ perfectly electrically conducting plate

scattered field from time-domain to frequency-domain. We therefore construct a subset of the original currents **J** as

$$\mathbf{J}_{f_d}^{\Delta f}(\mathbf{r}) = \int_{f_d-\frac{\Delta f}{2}}^{f_d+\frac{\Delta f}{2}} \mathbf{J}'(\mathbf{r}, f)\, df \tag{6}$$

The resolution in the frequency domain is therefore based solely on the choice of Δf. As usual, the scattered field (for the chosen range of Doppler shift) is found by employing $\mathbf{J}_{f_d}^{\Delta f}(\mathbf{r})$ in the radiation integral. Since the currents upon the geometry can be calculated for any given time, we note that unlike traditional signal processing methods, the user's arbitrary choice of time and frequency allows for any desirable resolution within the DTFD.

3. EXAMPLE

Geometry

As an example, we present the TFD generated by a 0.3λ × 5.0λ metallic plate rotating in the xy plane about the center at one end (see Fig. 3). The incident field is a plane wave in the xy plane and traveling along the positive x-axis.

To compute the DTFD, currents are first evaluated via the moment method at each look angle. The currents are then modified using Eqs. (5) and (6). Since the plate rotates about the origin, the velocity of the geometry at a given point **r** is

$$\mathbf{v}(\mathbf{r}) = 2\pi|\mathbf{r}|\hat{\phi} \tag{7}$$

where **v** is then substituted in (5). For reference, the monostatic RCS of the geometry (as it moves through a rotation of 360°) is shown in Figure 4(a). Note the sharp specular response at 90° and 270° and the broader traveling wave responses at about 20°, 160°, 200°, and 340°. The corresponding discrete Fourier transform of the scattered field is given in Figure 4(b), showing all frequencies present throughout the plate's entire rotation.

From (7) and Figure 4(b), we observe that the maximum Doppler frequency is ±63 Hz, occuring when the blade is at 90° and 270°, respectively. Thus, a well-formed TFD should give us some physical insight into these behaviors.

Figure 5 shows the TFD of the plate using the spectrogram method described above. From this image, we can clearly see the large specular and traveling wave returns but the physics of the behavior are unclear, largely due to the "smearing" in both time- and frequency-domain resulting from the uncertainty principle. Overall, the image doesn't show much more detail than the RCS plot of Figure 4(a).

Figure 6 shows the TFD of the plate using the proposed DTFD method with $\Delta f = (f_{\max} - f_{\min})/300 = 0.42$ Hz. In this graph, one can clearly see that the large traveling-wave returns are caused by 10 discrete scattering centers distributed along the outer portions of the blade. As one might expect, these ten discrete scattering centers correspond to the ten λ/2 sections ($10 \cdot \lambda/2 = 5\lambda$) of

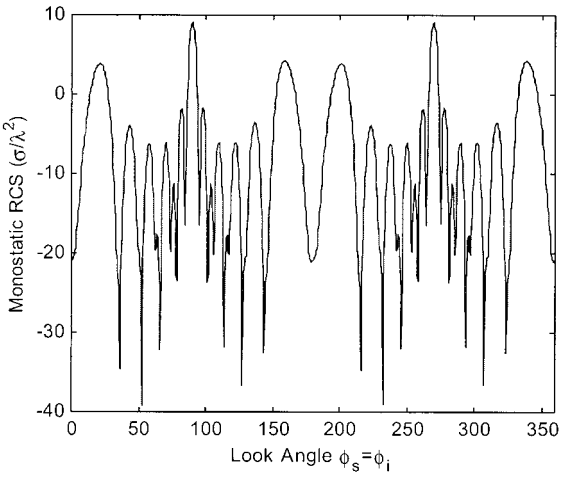

(a)

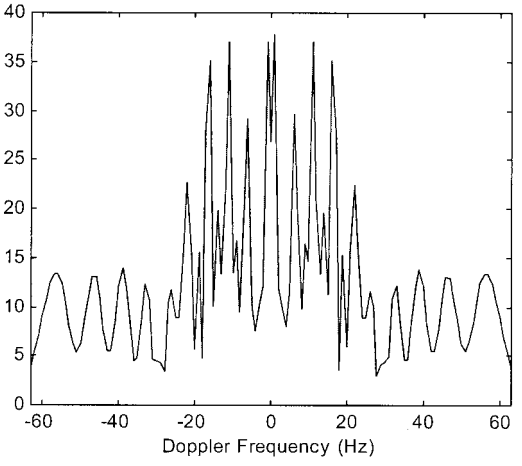

(b)

Figure 4 RCS of PEC plate in (a) time-domain. (b) Frequency-domain

the blade. Another curious feature is the apparent absence of the large specular return generated by the spectrogram in Figure 5. However, it is not difficult to conclude that the specular returns are

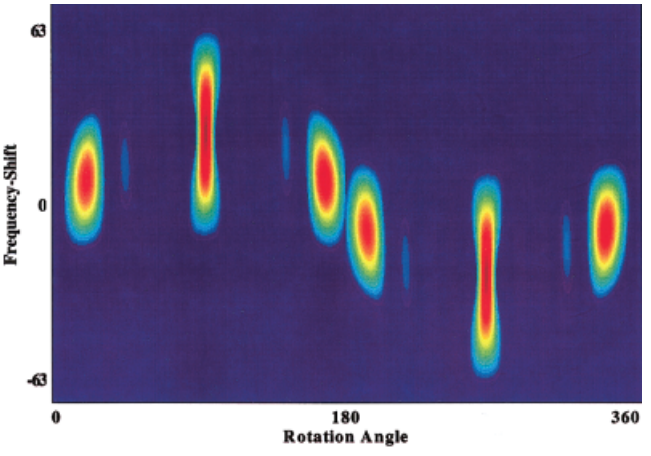

Figure 5 TFD of a spinning 5.0λ metallic plate generated by the spectrogram method [Color figure can be viewed in the online issue, which is available at www.interscience.wiley.com]

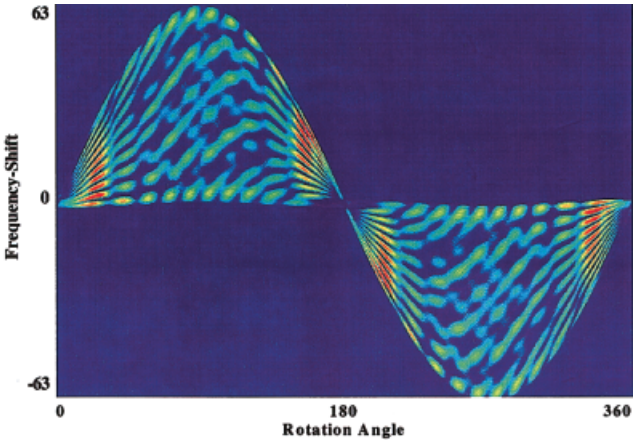

Figure 6 Direct TFD of a spinning 5.0λ metallic plate [Color figure can be viewed in the online issue, which is available at www.interscience.wiley.com]

created by the in-phase summation of many relatively small current elements located along the entire leading-edge of the blade—thus, the energy of the specular return is spread evenly along the entire blade and therefore appears at all Doppler frequencies. The spectrogram result suggests, incorrectly, that the specular return is caused largely by currents located at the center of the blade. Obviously this is not true and is a direct result of the uncertainty principle.

4. CONCLUSION

We presented the new Direct TFD method for generating TFD graphs with arbitrary resolution using only the computed currents and knowledge of the velocity of the geometry at each time step. The TFD of a spinning metallic plate was computed to demonstrate the much higher resolution of the proposed approach.

REFERENCES

1. R. Klemm, Space-time adaptive processing principles and applications, IEE, London, 1998.
2. C.J. McCormack, V.V. Liepa, and W.J. Williams, Applying time-frequency techniques to noise corrupted radar signals, IEEE Radar Conf Proc (1996), 345–350.
3. L. Cohen, Time-frequency distributions—A review, Proc IEEE 7 (1989), 941–981.
4. D.A. Dunavant, High degree efficient symmetrical gaussian quadrature rules for the triangle, Int J Num Meth Eng (1985), 1129–1148.
5. M. Carr, J.L. Volakis, and D.C. Ross, New time-frequency techniques for identification and extraction of scattering mechanisms, IEEE APS Int Symp (1998), 346–349.

DESIGN AND FABRICATION OF A SINGLE-ENDED GATE MIXER FOR A DOWN-CONVERTER IN WIRELESS APPLICATIONS

Dooyeong Yang[1] and You Chung Chung[2]
[1] Telecommunications and Computer Engineering
Cheju National University, Jeju, Korea
[2] Electrical and Computer Engineering
Utah State University, Logan, UT 84322-4120

Received 8 April 2002

ABSTRACT: *A single-ended gate mixer with a high conversion gain, low dissipated power, wide dynamic range and good isolation factor is designed and tested. The mixer is composed of a hairpin-line band-pass filter, an input/output matching circuit, a GaAs MESFET transistor, and a lumped element low-pass filter to convert the radio frequency (RF) into an intermediate frequency (IF). In the non-linearity analysis of a GaAs MESFET, the novel method with a harmonic balance technique is used to analyze the operating characteristics of a mixer circuit. The designed mixer outperforms a general mixer for a down converter in wireless applications.* © 2002 Wiley Periodicals, Inc. Microwave Opt Technol Lett 35: 189–193, 2002; Published online in Wiley InterScience (www.interscience.wiley.com). DOI 10.1002/mop.10553

Key words: *GaAs MESFET; mixer; MESFET mixer*

1. INTRODUCTION

The performance and the sensitivity of a receiver in a wireless local application are largely dependent on the mixer throughout in the microwave frequency range. A mixer is used as a nonlinear device to achieve frequency conversion of the input signal (radio frequency, RF) into the intermediate frequency (IF). A microwave diode or a field effect transistor (FET) is most commonly used as the nonlinear element in a mixer [1, 2]. Recently, a low-noise and high power GaAs MESFET transistor is being used in the microwave frequency band to improve the noise figure (NF) of the system. The MESFET mixer utilizes the non-linearity in the transconductance, the capacitance in the gate-source and the conductance in the drain-source of a MESFET to generate an output spectrum, consisting of the sum and the difference signal of the RF and the local oscillator (LO) signals. To analyze the non-linearity of the MESFET mixer accurately, Curtice used the harmonic balance technique with Newton's method [3]. The references [4] and [5] describe many advantages of the circuit simulators using the harmonic balance technique. The harmonic technique is also compared with the time domain simulation using SPICE [6]. Furthermore, Camacho-penalosa [7] utilized the Newton-Raphson algorithm for the nonlinear analysis with an improved harmonic balance technique using Jacobian partial derivatives to reduce the computing time of the MESFET gate mixer. The Serenade simulator [8] using the harmonic balance technique is used for analyzing the non-linearity characteristics of the GaAs MESFET mixer in this paper.

This paper presents a composite technique for designing a single-ended gate mixer having an excellent performance (with high conversion gain, low dissipated power, wide dynamic range and good isolation factor between ports) with low local power levels using a GaAs MESFET. To obtain these excellent performances, this mixer consists of a hairpin-line band-pass filter (BPF), two input/output matching circuits, a GaAs MESFET and a Tchebycheff low-pass filter (LPF). A general mixer has an IF amplifier at the IF port, but this mixer proposed in this paper does